RSC Advances

PAPER

View Article Online
View Journal | View Issue

Cite this: *RSC Adv.*, 2017, **7**, 55986

Effects of the additives *n*-propylammonium or *n*-butylammonium iodide on the performance of perovskite solar cells†

Cheng-Ming Hsieh,[a] Yen-Lin Yu,[b] Chih-Ping Chen *[b] and Shih-Ching Chuang *[a]

Organic–inorganic lead halide perovskite solar cells (PSCs) offer a promising low-cost manufactural solar technology as they are compatible with large-scale and low-temperature (<100 °C) solution processes. Through the optimization of perovskite active layer and phenyl-C_{61}-butyric acid methyl ester ($PC_{61}BM$) layer thickness, the normal cells showed 9.7% power conversion efficiency (PCE). Compared with the corresponding normal devices, we observed an improvement in PCE from 9.7% to 11.3% and 10.2% for the devices prepared using 1 vol% of $C_3H_7NH_3I$ and 1 vol% of $C_4H_9NH_3I$ as additives, respectively. *Via* analysis by ultraviolet-visible (UV-vis) spectroscopy, grazing incidence wide angle X-ray diffraction (GIWAXS), and field emission scanning electron microscopy (FE-SEM), we concluded that the morphological changes, absorption, and crystallinity of the perovskite films played an important role that influenced the performance of the PSC devices with various additives. The presence of 1% of $C_3H_7NH_3I$ or 1% of $C_4H_9NH_3I$ caused the $CH_3NH_3PbI_{3-x}Cl_x$ films to grow uniformly with high coverage and continuous phase, as well as with higher absorption; this enabled the corresponding devices to display improved performance.

Received 13th October 2017
Accepted 27th November 2017

DOI: 10.1039/c7ra11286f

rsc.li/rsc-advances

Introduction

Perovskite solar cells (PSCs) demonstrate many advantages, including low-cost solution process, thin film, and high power conversion efficiencies (PCEs), and their PCE has been engineered to increase from 3.8% to 22% within only 8 years.[1–6] This technology has demonstrated considerable prospects in achieving efficiency comparable to or even better than those of other thin-film solar cells (CIGS and CdTe). However, rendering PSCs toward commercialization with long-term stability is challenging since the perovskite materials are sensitive towards atmosphere, humidity, and temperature. In general, PSCs are actually fabricated at temperatures above 50 °C, and the perovskites may degrade over time.[7–14] To obtain high performance PSCs, it is important to produce a high-quality thin film since the photoelectric characteristics and the surface topography are governed by the morphology. The crystallization behaviour of the perovskite thin films controls the development of surface topography, which affects the charge separation, recombination mechanics, and diffusion-length of perovskite thin films. Key factors, including deposition method, surrounding, precursor composition, solvent,[15–21] and the additives used, control the crystallization process.[18,22–28] PSCs with a PCE of more than 20% relied on process modification and material engineering.[29] Using a simple perovskite solution deposition method, the mesoporous scaffold provides physical limitations on the size of the perovskite crystals to achieve the desired quality of the relative thickness film. Thus, it is necessary to have better charge transport with larger perovskite grains.[30] The crystallization kinetics of the films grown on the planar structure are different from that of the mesoporous scaffolds because the lack of mesoporous scaffolds and the reduced surface energy of the perovskite precursors will result in less nucleation sites. The process of homogeneous crystallization consists of two steps: nucleation and growth. Non-ideal surface energy can lead to Volmer–Weber growth, which is due to the rapid growth of perovskite thin films that leads to discontinuous films with large size grains accompanied by many pores.[31] Therefore, the key solution is the development of perovskite crystal manipulation that controls nucleation and growth effectively to achieve the best film morphology and crystallinity.[32–45] The addition of a small amount of chemical additives has been demonstrated as an efficient way to tailor the morphology of perovskite thin film, including broad coverage and enhanced crystallinity, thereby enhancing the performance of the devices.[46,47] Liang *et al.* observed that the addition of 1,8-diiodooctane (DIO) as an additive[32] made the surface morphology of the perovskite thin film denser; thus, the performance of the devices was improved. Recently, 2D

[a]*Department of Applied Chemistry, National Chiao Tung University, Hsinchu, Taiwan, Republic of China. E-mail: jscchuang@faculty.nctu.edu.tw*

[b]*Department of Materials Engineering, Ming Chi University of Technology, New Taipei City, Republic of China. E-mail: cpchen@mail.mcut.edu.tw*

† Electronic supplementary information (ESI) available. See DOI: 10.1039/c7ra11286f

perovskites, obtained by inserting bulky alkylammonium cations in between anionic layers, have shown increased solar cell stability.[48,49] We have used ethylammonium iodide (EAI) as an additive in our previous study and observed an enhancement of PCE (9.4 ± 0.76 to 10.2 ± 0.58%) and long term stability of the PSC. The EAI-derived device retained *ca.* 80% of the PCEs under accelerated heating (65 °C) inside glove box for over 360 h.[50] In this study, we doped the perovskite layer with alkylammonium salts, *i.e.* *n*-propylammonium (0.24 nm) and *n*-butylammonium (0.26 nm) iodides, having greater ionic radius.[51] Recently, Snaith and coworkers have studied the incorporation of *n*-butylammonium iodide into the caesium–formamidinium lead halide perovskite and observed plate-like crystallites standing up between the 3D perovskite grains, and this has dramatically enhanced the device stability.[52] The embedding of $C_3H_7NH_3I$ (PAI) and $C_4H_9NH_3I$ (BAI) as additives may lead to deformation and twisting of the lattice of perovskites; as a result, we may slow the rate of crystallization of perovskite thin film and form a flat surface with less pinholes, thereby promoting the formation of the preferred surface topography that allows efficient free carrier transportation.

Experimental

Materials and methods

All chemicals were purchased from Aldrich and used as received, unless otherwise specified. MAI, PAI, and BAI were synthesized according to previously reported techniques.[50] *N*-Propylamine or *n*-butylamine (2.0 M in MeOH, Aldrich) and hydroiodic acid (57% w/w aq. soln, stabilized with 1.5% hypophosphorous acid, Alfa Aesar) were stirred at 0 °C under N_2 for 2 h. The solvent was evaporated in a rotary evaporator under vacuum. The crude residue was dissolved in MeOH (5 mL) and poured into Et_2O (200 mL). The precipitate was obtained and dried under vacuum to afford PAI and BAI as a white product. The detailed experimental and fabricated conditions are shown in the ESI.†

Results and discussion

From the UV-vis absorption spectra shown in Fig. 1, we observed enhancement of the absorption intensities for the perovskite thin films with optimized $C_3H_7NH_3I$ and $C_4H_9NH_3I$ as additives. Upon adding 1% and 2.5% of $C_3H_7NH_3I$ and $C_4H_9NH_3I$, absorption in the 300–400 nm region showed significant enhancement. Thus, we infer that the perovskite thin film surface morphology and coverage may become better with the addition of these two additives. Furthermore, according to grazing incidence wide angle X-ray diffraction (GIWAXS) analysis in Fig. 2, the addition of $C_3H_7NH_3I$ and $C_4H_9NH_3I$ as additives does not give rise to extra diffraction peaks; this indicates that the addition of these two additives in these concentrations does not cause significant changes in the perovskite structure. In this study, the GIWAXS images were plotted with the *x*-axial of the scattering vector q (equals to $4\pi \sin\theta/\lambda$; herein, θ refers to the half of the total scattering angle with λ at the wavelength of 0.145 nm). The scattering peak

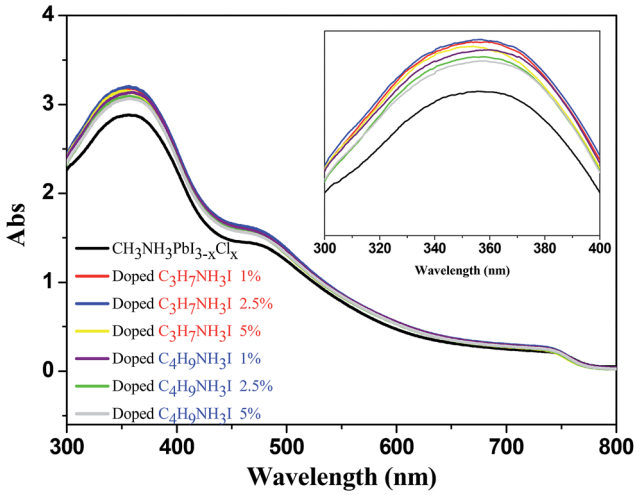

Fig. 1 UV-vis absorption spectra for perovskite thin films obtained after doping with various concentration of $C_3H_7NH_3I$ and $C_4H_9NH_3I$.

appearing at the *q* of 10 nm^{-1} belongs to the scattering peak of the (110) plane of $CH_3NH_3PbI_{3-x}Cl_x$ perovskite structure.[53] We observed no characteristic peaks of MAI and $PbCl_2$, and the peak for the precursor structure of perovskite at a value of *q* of 11 nm^{-1} disappears; this indicates the complete crystallization of perovskite for the studied condition. It was also found that the intensity of the (110) characteristic peaks varied with the addition of different additives; thus, it was further deduced that the crystal sizes of different additives could vary with the amount of additives, thereby affecting the grain nucleation and growth.

We used the GIWAXS data to calculate the individual half-width and then used the Scherrer formula to determine the grain size. As summarized in Table 1, it was found that the grain sizes did not change significantly upon the addition of 1%, 2.5%, and 5% of $C_3H_7NH_3I$, as well as 1% and 2.5% of $C_4H_9NH_3I$, whereas the grain sizes became obviously smaller,

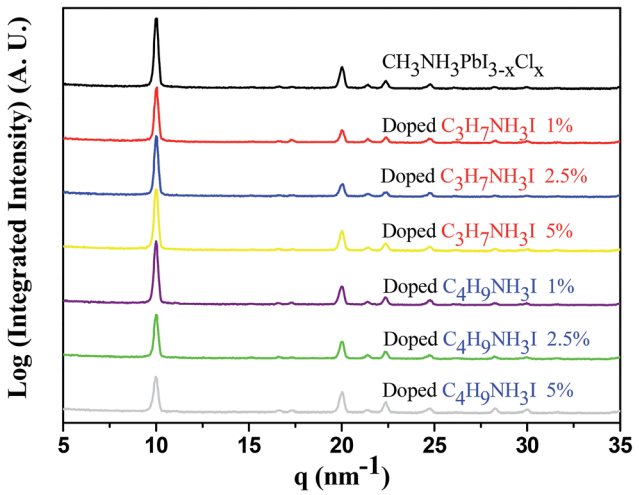

Fig. 2 XRD pattern of the perovskite thin films obtained after doping with various concentrations of $C_3H_7NH_3I$ and $C_4H_9NH_3I$.

Table 1 Variation of perovskite thin film grain size after doping with $C_3H_7NH_3I$ and $C_4H_9NH_3I$

Doping	Full width at half maximum	Grain size
$CH_3NH_3PbI_{3-x}Cl_x$	0.38	20.8 nm
$C_3H_7NH_3I$ 1%	0.38	20.8 nm
$C_3H_7NH_3I$ 2.5%	0.38	20.8 nm
$C_3H_7NH_3I$ 5%	0.39	20.8 nm
$C_4H_9NH_3I$ 1%	0.39	20.8 nm
$C_4H_9NH_3I$ 2.5%	0.39	20.8 nm
$C_4H_9NH_3I$ 5%	0.41	19.3 nm

with 19.3 nm size, upon the addition of 5% of $C_4H_9NH_3I$. This indicates that the addition of more large ionic species as additives affects the grain sizes; thus, the perovskite precursors affect the formation of the perovskite layer.

For an optimized perovskite layer, the high coverage is critical to determine the performance of PSC. Fig. S1† displays the SEM image of the normal perovskite thin film; it can be observed that the surface morphology contains irregular sizes of hole with coverage of about 93.1%. We also observed the discontinuity of the grain boundaries for this film. As shown in Fig. 3(a), (a-1) and (a-2), upon the addition of 1%, 2.5%, and 5% $C_3H_7NH_3I$ as additives, respectively, the pores on the film surface were significantly reduced, and the grain boundary became more continuous with coverage increased up to 97.4%, 97.6%, and 97.5%. As shown in Fig. 3(b), (b-1) and (b-2), the addition of 1%, 2.5%, and 5% $C_4H_9NH_3I$ resulted in increased coverage of upto 96.2%, 95.8%, and 95.7%, respectively. As a result, the addition of $C_3H_7NH_3I$ and $C_4H_9NH_3I$ as additives make the perovskite thin film more flat with reduction of size and number of the pores. As reflected in their UV-vis spectra, the films with a higher rate of coverage exhibited stronger absorption in the visible region. By adding 10% of $C_3H_7NH_3I$ and $C_4H_9NH_3I$, the excess additives result in a change of the surface topographies; as shown in Fig. 3(a-3) and (b-3), we observed large amount of pores for these films. This indicated that limited light harvesting and irregular grain may impede the free carrier transport in the interface. Based on the SEM images and UV-vis and XRD analyses, we concluded that the addition of optimized ratios of $C_3H_7NH_3I$ and $C_4H_9NH_3I$ helped the crystalline perovskite formation with higher coverage, *i.e.*, reduction of pores, and made the surface morphology more flat. Thus, more efficient electron and hole transport may occur and enhance the performance of the devices. An optimized annealing time for our normal (no PAI or BAI) and PAI and BAI-derived perovskite films was 2.5 and 3.5 h, respectively. Due to the greater ionic radius of propyl and butyl cation when compared with that of methyl-based ammonium iodide, the incorporation of these additives slowed down the formation of the perovskite structure. Alternatively, the embedding of bulky ammonium cations may form the 2D perovskites, and these structures can form a self-assembly structure, and typically, a smoother surface is exhibited.[49] Based on these reasons, we observed the perovskites growing into a flat surface with a higher coverage as well as higher absorbance.

The performance of the PSC devices doped with $C_3H_7NH_3I$ and $C_4H_9NH_3I$ is summarized in Table 2. The pre-optimized PSC cells showed an average PCE of 8.4 ± 1.6% with the highest value of 9.7%, along with the value of J_{sc} of 18.1 mA cm^{-2}, a value of open circuit voltage (V_{oc}) of 0.88 V and a fill factor (FF) value of 60.6%. The PCEs of devices doped with 1%, 2.5%, and 5% of $C_3H_7NH_3I$ were 10.2 ± 1.1%, 10.4 ± 0.9%, and 10.2 ± 0.5%, respectively (Fig. 4). The PCEs of $C_4H_9NH_3I$-derived devices with concentration of 1%, 2.5%, and 5% of $C_3H_7NH_3I$ were 9.9 ± 0.3%, 10.0 ± 0.1%, and 9.3 ± 0.6%, respectively (Fig.

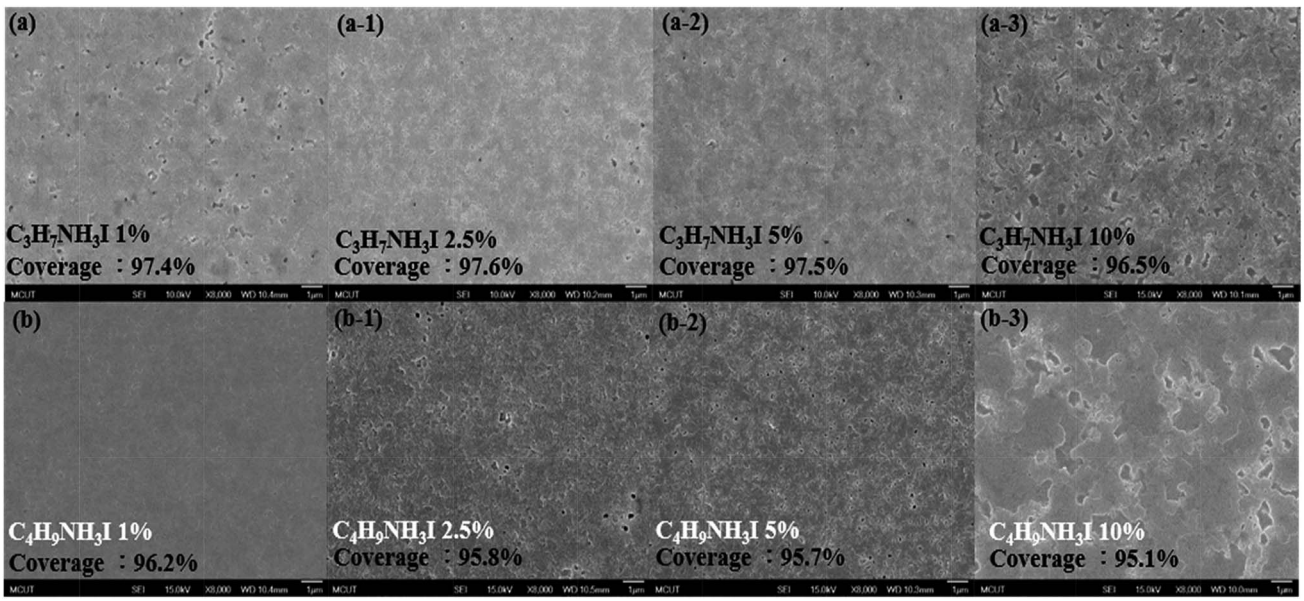

Fig. 3 FE-SEM images of $CH_3NH_3PbI_{3-x}Cl_x$ perovskite thin films doped with different concentration of (a) to (a-3) $C_3H_7NH_3I$ and (b) to (b-3) $C_4H_9NH_3I$ precursors; magnification by 8000 times.

Table 2 PV parameters of PVSK devices upon doping $C_3H_7NH_3I$ and $C_4H_9NH_3I$

Doping	J_{sc} (mA cm^{-2})	V_{oc} (V)	FF (%)	PCE (%)	Best PCE (%)	R_{sh} (Ω cm^2)	R_s (Ω cm^2)
$CH_3NH_3PbI_{3-x}Cl_x$	18.1	0.88	60.6	8.4 ± 1.6	9.7	316.4	11.3
$C_3H_7NH_3I$ 1%	18.7	0.89	68.0	10.2 ± 1.1	11.3	471.5	9.3
$C_3H_7NH_3I$ 2.5%	17.9	0.99	63.8	10.4 ± 0.9	11.3	428.9	13.5
$C_3H_7NH_3I$ 5%	17.8	0.92	64.8	10.2 ± 0.5	10.6	443.2	13.4
$C_4H_9NH_3I$ 1%	18.3	0.92	60.8	9.9 ± 0.3	10.2	316.3	11.1
$C_4H_9NH_3I$ 2.5%	17.4	0.93	62.2	10.0 ± 0.1	10.1	401.7	15.2
$C_4H_9NH_3I$ 5%	17.6	0.93	61.1	9.3 ± 0.6	10.0	318.8	13.9

5). We observed the highest PCE of 11.3% for the device with 2.5% of $C_3H_7NH_3I$ additive, with a J_{sc} of 17.9 mA cm^{-2}, a value of V_{oc} of 0.99 V, and an FF value of 63.8%, which was increased by 16.5% when compared with that of the pre-optimized normal devices. It was observed that V_{oc} and FF values significantly increased after doping with 1%, 2.5%, and 5% of $C_3H_7NH_3I$; this indicated that the perovskite thin film after doping with $C_3H_7NH_3I$ produced a good surface morphology because the reduction of holes could effectively reduce the chance of contact between the hole transport layer and the electron transport layer and thus avoid the occurrence of a free carrier recombination or a low V_{oc}. Moreover, the perovskite thin film has good contact with the hole transport layer (PEDTO:PSS) and the electron transport layer (PCBM), producing better charge separation and transfer effect; thus, the PCE of the PSC device is improved. It was found that the addition of these additives not only increased the device performance but also improved the reproducibility of the device efficiency – the variation in the PCE was small. *Via* observation from the UV-vis measurement and FE-SEM coverage, the absorption intensity and coverage are relatively high with doped devices. Therefore, after doping $C_3H_7NH_3I$ and $C_4H_9NH_3I$ into the devices, the power conversion efficiency was excellent.

We calculated the series (R_s) and shunt (R_{sh}) resistances from the respective *J*–*V* curves. The values of R_{sh} and R_s of the $C_3H_7NH_3I$-based devices are 471.5 and 9.3 Ω cm^2, respectively, whereas for the $C_4H_9NH_3I$-based devices, they are 401.7 and 15.2 Ω cm^2, respectively. Moreover, for $CH_3NH_3PbI_{3-x}Cl_x$-based devices, they are 316.4 and 11.3 Ω cm^2 for R_{sh} and R_s values, respectively. The value of R_s of a perovskite device is related to the resistance of the perovskite thin film, the interfacial contact resistance for all layers, and the resistance of the electrode contacts. The resistance of the perovskite thin film may relate to its morphology, grain size, and surface coverage. The corresponding greater values of R_{sh} for the $C_3H_7NH_3I$-based devices suggest lower leakage currents and fewer defects for charge recombination loss. Based upon FE-SEM study, the perovskite thin film with $C_3H_7NH_3I$ as additives exhibited higher rate of coverage than those with $C_4H_9NH_3I$ doped and normal $CH_3NH_3PbI_{3-x}Cl_x$. These devices with $C_3H_7NH_3I$ as additives showed delicate textures with less pin holes. It was worthy to note that delicate thin film generally exhibited higher FF values and associated with larger R_{sh} and smaller R_s values. This notion was reflected from the FF, R_{sh}, and R_s values in Table 2. The perovskite device with $C_3H_7NH_3I$ as additives showed relatively large (471.5 Ω cm^2) and smaller R_s (9.3 Ω cm^2) and those with $C_4H_9NH_3I$ and $CH_3NH_3PbI_{3-x}Cl_x$ exhibited R_{sh} of 401.7 Ω cm^2 and R_s of 15.2 Ω cm^2 as well as R_{sh} of 316.4 Ω cm^2 and R_s of 11.3 Ω cm^2, respectively. The device with $C_3H_7NH_3I$ as additives showed best FF value (68.0%)—this value was greater

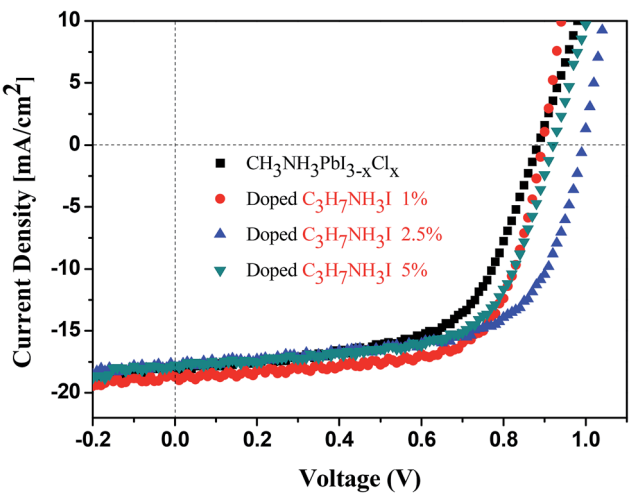

Fig. 4 The *J*–*V* curve with doped $C_3H_7NH_3I$ devices.

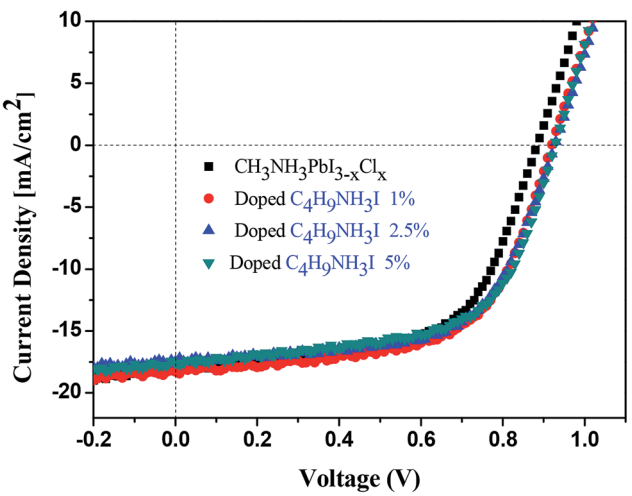

Fig. 5 The *J*–*V* curve with $C_4H_9NH_3I$-doped devices.

than those of the devices with $C_4H_9NH_3I$ (62.2%) and $CH_3NH_3PbI_{3-x}Cl_x$ (60.6%).

We further investigated the device stability in the presence of various concentrations of $C_3H_7NH_3I$ and $C_4H_9NH_3I$ and compared it to that of the normal devices. To eliminate the factor of the uncertainty of encapsulation, we determined the stability of the device inside the glove box at room temperature (~25 °C). As shown in Fig. 6, the performance of normal device on the seventh day reduced to 95% or less as compared to the PCE on the first day of the measurement. The addition of $C_3H_7NH_3I$ as additives helped in the stability of devices. In a previous report, Boschlo and coworkers used XRD to demonstrate the transformation of perovskite film from less order structure to more crystalline after storage at room temperature under inert gas.[54] The initial increase in PCE of $C_3H_7NH_3I$ 2.5%-based PSC device after storage at room temperature inside N_2 filled glove box might arise from the enhancement of the crystallinity of the perovskite film.[53] The PCE of normal devices measured on the 49th day has been reduced to 80%; however, those with 1%, 2.5%, and 5% of $C_3H_7NH_3I$ in the devices maintain PCE at 88%, 93%, and 86% on the 49th day. This notion indicated that addition of $C_3H_7NH_3I$ as additives can improve the stability of the devices. Moreover, one typical doping with 2.5% of $C_3H_7NH_3I$ provided superior stability over the degradation test. Furthermore, as shown in Fig. 7, the addition of $C_4H_9NH_3I$ as additives helped device stability more than that upon the addition of $C_3H_7NH_3I$. By addition of 1%, 2.5%, and 5% of $C_4H_9NH_3I$ as additives to the devices, the PCE of devices were maintained at 89%, 93%, and 98% efficiency, respectively, on the 49th day, which indicated that addition of $C_4H_9NH_3I$ could improve the stability of the device greatly. It is recently evidenced that Ruddlesden–Popper 2D perovskites have shown to appeal improved stability.[55] Typically, 2D perovskites are formed through the embedding of large and bulky alkylammonium cations.[49,52] It is possible that a partial 2D perovskite structure may appear in the PAI and BAI-doped perovskite and cause the enhancement of the stability.

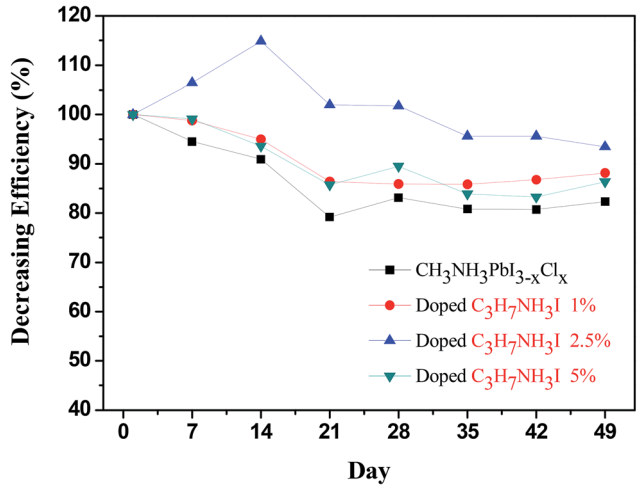

Fig. 6 The stability of devices with $C_3H_7NH_3I$ doping.

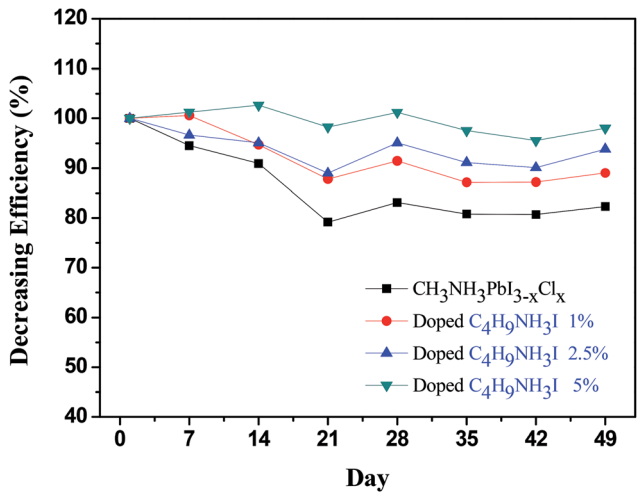

Fig. 7 The stability of devices with $C_4H_9NH_3I$ doping.

Conclusion

We have demonstrated that small amounts of alkylammonium iodides ($C_3H_7NH_3I$ and $C_4H_9NH_3I$) in the perovskite precursor solution can improve the surface morphology and crystallinity of the perovskite thin films. It could effectively increase the efficiency of the PSC devices from 9.7% to 11.3% and 10.2%. This can be clearly observed in the UV-vis spectra since the change of the surface morphology can increase the absorption intensity of perovskite, indicating that perovskites exhibit good surface morphology after incorporation of additives. From the XRD and SEM analysis, it was proven that the addition of additives could make homogeneous nucleation and the crystallinity of perovskite thin film more continuous with decreased porosity. By enhancing the crystallinity and the improvement of the surface morphology, the charge transfer efficiency between the perovskite layer and the charge transport layers can be improved. Both $C_3H_7NH_3I$ and $C_4H_9NH_3I$-doped devices have the effect of improving the reproducibility and efficiency. Thus, $C_3H_7NH_3I$- and $C_4H_9NH_3I$-doped devices have excellent performance and can effectively improve the efficiency and stability of the PSCs.

Conflicts of interest

There are no conflicts to declare.

Acknowledgements

We thank the Ministry of Science and Technology of Taiwan (MOST 106-2113-M-131-001-MY2; MOST 105-2221-E-131-033-) for providing the financial support.

References

1 A. Kojima, K. Teshima, Y. Shirai and T. Miyasaka, *J. Am. Chem. Soc.*, 2009, **131**, 6050–6051.
2 NREL, 20170117.
3 X. Liu, F. Lin, C.-C. Chueh, Q. Chen, T. Zhao, P.-W. Liang, Z. Zhu, Y. Sun and A. K. Y. Jen, *Nano Energy*, 2016, **30**, 417–425.
4 J. Cheng, X. Ren, H. L. Zhu, J. Mao, C. Liang, J. Zhuang, V. A. L. Roy and W. C. H. Choy, *Nano Energy*, 2017, **34**, 76–85.
5 P.-L. Qin, Q. He, C. Chen, X.-L. Zheng, G. Yang, H. Tao, L.-B. Xiong, L. Xiong, G. Li and G.-J. Fang, *Solar RRL*, 2017, **1**, 1700058.
6 L. Meng, E.-P. Yao, Z. Hong, H. Chen, P. Sun, Z. Yang, G. Li and Y. Yang, *Adv. Mater.*, 2017, **29**, 1603826.
7 J. He, C. F. Ng, K. Y. Wong, W. F. Liu and T. Chen, *Chempluschem*, 2016, **81**, 1292–1298.
8 L. Kavan, L. Steier and M. Gratzel, *J. Phys. Chem. C*, 2017, **121**, 342–350.
9 A. G. Kontos, A. Kaltzoglou, E. Siranidi, D. Palles, G. K. Angeli, M. K. Arfanis, V. Psycharis, Y. S. Raptis, E. I. Kamitsos, P. N. Trikalitis, C. C. Stoumpos, M. G. Kanatzidis and P. Falaras, *Inorg. Chem.*, 2017, **56**, 84–91.
10 M. Kot, C. Das, Z. P. Wang, K. Henkel, Z. Rouissi, K. Wojciechowski, H. J. Snaith and D. Schmeisser, *Chemsuschem*, 2016, **9**, 3401–3406.
11 X. D. Liu, P. Huang, Q. Q. Dong, Z. W. Wang, K. C. Zhang, H. Yu, M. Lei, Y. Zhou, B. Song and Y. F. Li, *Sci. China: Chem.*, 2017, **60**, 136–143.
12 M. A. Mahmud, N. K. Elumalai, M. B. Upama, D. Wang, F. Haque, M. Wright, K. H. Chan, C. Xu and A. Uddin, *Phys. Status Solidi RRL*, 2016, **10**, 882–889.
13 H. F. Yang, J. C. Zhang, C. F. Zhang, J. J. Chang, Z. H. Lin, D. Z. Chen, X. Sun, H. Xi, G. Q. Han and Y. Hao, *Sol. Energy*, 2016, **139**, 190–198.
14 X. J. Zheng, C. C. Wu, S. K. Jha, Z. Li, K. Zhu and S. Priya, *ACS Energy Lett.*, 2016, **1**, 1014–1020.
15 A. Dubey, E. A. Gaml, N. Adhikari, K. M. Reza, H. Zeyada, Q. Q. Qiao and Ieee, in *2016 Ieee International Conference on Electro Information Technology*, 2016, pp. 716–722.
16 G. P. Li, H. Wang, T. Zhang, L. F. Mi, Y. G. Zhang, Z. P. Zhang, W. J. Zhang and Y. Jiang, *Adv. Funct. Mater.*, 2016, **26**, 8478–8486.
17 Y. F. Wang, S. B. Li, P. Zhang, D. T. Liu, X. L. Gu, H. Sarvari, Z. B. Ye, J. Wu, Z. M. Wang and Z. D. Chen, *Nanoscale*, 2016, **8**, 19654–19661.
18 L. Xie, H. Hwang, M. Kim and K. Kim, *Phys. Chem. Chem. Phys.*, 2017, **19**, 1143–1150.
19 Q. Y. Xu, D. X. Yuan, H. R. Mu, F. Igbari, Q. L. Bao and L. S. Liao, *Nanoscale Res. Lett.*, 2016, **11**, 248.
20 Y. Yu, S. W. Yang, L. Lei, Q. P. Cao, J. Shao, S. Zhang and Y. Liu, *ACS Appl. Mater. Interfaces*, 2017, **9**, 3667–3676.
21 Z. C. Yuan, Y. G. Yang, Z. W. Wu, S. Bai, W. D. Xu, T. Song, X. Y. Gao, F. Gao and B. Q. Sun, *ACS Appl. Mater. Interfaces*, 2016, **8**, 34446–34454.
22 B. J. Foley, J. Girard, B. A. Sorenson, A. Z. Chen, J. S. Niezgoda, M. R. Alpert, A. F. Harper, D. M. Smilgies, P. Clancy, W. A. Saidi and J. J. Choi, *J. Mater. Chem. A*, 2017, **5**, 113–123.
23 S. N. Habisreutinger, N. K. Noel, H. J. Snaith and R. J. Nicholas, *Adv. Energy Mater.*, 2017, **7**, DOI: 10.1002/aenm.201601839.
24 X. M. Hou, Y. Hu, H. W. Liu, A. Y. Mei, X. Li, M. Duan, G. A. Zhang, Y. G. Rong and H. W. Han, *J. Mater. Chem. A*, 2017, **5**, 73–78.
25 J. Liang, C. X. Wang, Y. R. Wang, Z. R. Xu, Z. P. Lu, Y. Ma, H. F. Zhu, Y. Hu, C. C. Xiao, X. Yi, G. Y. Zhu, H. L. Lv, L. B. Ma, T. Chen, Z. X. Tie, Z. Jin and J. Liu, *J. Am. Chem. Soc.*, 2016, **138**, 15829–15832.
26 C. J. Qin, T. Matsushima, T. Fujihara and C. Adachi, *Adv. Mater.*, 2017, **29**, DOI: 10.1002/adma.201603808.
27 Y. Yu, C. L. Wang, C. R. Grice, N. Shrestha, J. Chen, D. W. Zhao, W. Q. Liao, A. J. Cimaroli, P. J. Roland, R. J. Ellingson and Y. F. Yan, *Chemsuschem*, 2016, **9**, 3288–3297.
28 Y. F. Yue, N. Salim, Y. Z. Wu, X. D. Yang, A. Islam, W. Chen, J. Liu, E. B. Bi, F. X. Xie, M. L. Cai and L. Y. Han, *Adv. Mater.*, 2016, **28**, 10738–10743.
29 M. Saliba, T. Matsui, J.-Y. Seo, K. Domanski, J.-P. Correa-Baena, M. K. Nazeeruddin, S. M. Zakeeruddin, W. Tress, A. Abate, A. Hagfeldt and M. Gratzel, *Energy Environ. Sci.*, 2016, **9**, 1989–1997.
30 J. H. Heo, S. H. Im, J. H. Noh, T. N. Mandal, C.-S. Lim, J. A. Chang, Y. H. Lee, H.-j. Kim, A. Sarkar and M. K. Nazeeruddin, *Nat. Photonics*, 2013, **7**, 486–491.
31 V. Burlakov, G. Eperon, H. Snaith, S. Chapman and A. Goriely, *Appl. Phys. Lett.*, 2014, **104**, 091602.
32 P. W. Liang, C. Y. Liao, C. C. Chueh, F. Zuo, S. T. Williams, X. K. Xin, J. Lin and A. K. Jen, *Adv. Mater.*, 2014, **26**, 3748–3754.
33 M. M. Lee, J. Teuscher, T. Miyasaka, T. N. Murakami and H. J. Snaith, *Science*, 2012, **338**, 643–647.
34 P. Docampo, J. M. Ball, M. Darwich, G. E. Eperon and H. J. Snaith, *Nat. Commun.*, 2013, **4**, 2761.
35 M. Liu, M. B. Johnston and H. J. Snaith, *Nature*, 2013, **501**, 395–398.
36 Z. Xiao, C. Bi, Y. Shao, Q. Dong, Q. Wang, Y. Yuan, C. Wang, Y. Gao and J. Huang, *Energy Environ. Sci.*, 2014, **7**, 2619.
37 Y. Song, S. Lv, X. Liu, X. Li, S. Wang, H. Wei, D. Li, Y. Xiao and Q. Meng, *Chem. Commun.*, 2014, **50**, 15239–15242.
38 T. Leijtens, B. Lauber, G. E. Eperon, S. D. Stranks and H. J. Snaith, *J. Phys. Chem. Lett.*, 2014, **5**, 1096–1102.
39 H. Zhou, Q. Chen, G. Li, S. Luo, T.-b. Song, H.-S. Duan, Z. Hong, J. You, Y. Liu and Y. Yang, *Science*, 2014, **345**, 542–546.
40 G. E. Eperon, V. M. Burlakov, P. Docampo, A. Goriely and H. J. Snaith, *Adv. Funct. Mater.*, 2014, **24**, 151–157.
41 J.-H. Im, H.-S. Kim and N.-G. Park, *APL Mater.*, 2014, **2**, 081510.
42 B. R. Sutherland, S. Hoogland, M. M. Adachi, P. Kanjanaboos, C. T. Wong, J. J. McDowell, J. Xu,

O. Voznyy, Z. Ning and A. J. Houtepen, *Adv. Mater.*, 2015, **27**, 53–58.

43 Q. Chen, H. Zhou, Z. Hong, S. Luo, H.-S. Duan, H.-H. Wang, Y. Liu, G. Li and Y. Yang, *J. Am. Chem. Soc.*, 2013, **136**, 622–625.

44 Z. Xiao, Q. Dong, C. Bi, Y. Shao, Y. Yuan and J. Huang, *Adv. Mater.*, 2014, **26**, 6503–6509.

45 N. J. Jeon, J. H. Noh, Y. C. Kim, W. S. Yang, S. Ryu and S. I. Seok, *Nat. Mater.*, 2014, **13**, 897–903.

46 C. Zuo and L. Ding, *Nanoscale*, 2014, **6**, 9935–9938.

47 C. Y. Chang, C. Y. Chu, Y. C. Huang, C. W. Huang, S. Y. Chang, C. A. Chen, C. Y. Chao and W. F. Su, *ACS Appl. Mater. Interfaces*, 2015, **7**, 4955–4961.

48 H. Tsai, W. Nie, J.-C. Blancon, C. C. Stoumpos, R. Asadpour, B. Harutyunyan, A. J. Neukirch, R. Verduzco, J. J. Crochet, S. Tretiak, L. Pedesseau, J. Even, M. A. Alam, G. Gupta, J. Lou, P. M. Ajayan, M. J. Bedzyk, M. G. Kanatzidis and A. D. Mohite, *Nature*, 2016, **536**, 312–316.

49 Y. Chen, Y. Sun, J. Peng, W. Zhang, X. Su, K. Zheng, T. Pullerits and Z. Liang, *Adv. Energy Mater.*, 2017, **7**, 1700162.

50 H. L. Hsu, C. C. Chang, C. P. Chen, B. H. Jiang, R. J. Jeng and C. H. Cheng, *J. Mater. Chem. A*, 2015, **3**, 9271–9277.

51 B. N. Cohen, C. Labarca, N. Davidson and H. A. Lester, *J. Gen. Physiol.*, 1992, **100**, 373–400.

52 Z. Wang, Q. Lin, F. P. Chmiel, N. Sakai, L. M. Herz and H. J. Snaith, *Nat. Energy*, 2017, **6**, 17135.

53 H.-L. Hsu, C.-P. Chen, J.-Y. Chang, Y.-Y. Yu and Y.-K. Shen, *Nanoscale*, 2014, **6**, 10281.

54 B.-w. Park, B. Philippe, T. Gustafsson, K. Sveinbjörnsson, A. Hagfeldt, E. M. J. Johansson and G. Boschloo, *Chem. Mater.*, 2014, **26**, 4466–4471.

55 L. Pedesseau, D. Sapori, B. Traore, R. Robles, H.-H. Fang, M. A. Loi, H. Tsai, W. Nie, J.-C. Blancon, A. Neukirch, S. Tretiak, A. D. Mohite, C. Katan, J. Even and M. Kepenekian, *ACS Nano*, 2016, **10**, 9776–9786.